Acta Technica *62* (2017), No. 7A, 1623–1634

A fault-tolerant control method for morphing aircraft based on multi-dimensional subspace map identification

Siyue Liang[1]

Abstract. In the process of aeromagnetic survey, it is necessary to install a high-precision magnetometer on the morphing aircraft. However, due to the inevitable existence of ferromagnetic and metal material on the morphing aircraft, as well as the variation of the course and moving posture of the morphing aircraft, a large interfering magnetic field of the non-detecting target will be produced. In order to eliminate this interference, a fault-tolerant control method for morphing aircraft based on multidimensional subspace map identification is proposed in this paper. First of all, by clarifying the basic principle of generation of magnetic interference , the types and properties of the interfering magnetic field generated in the process of aeromagnetic survey were analyzed, and the corresponding mathematical models were established; Secondly, the dynamic estimation of unknown equipment system model is done by using the same projection on the time offset set based on relevant data and the least square operation. Finally, the effectiveness of the proposed fault-tolerant control method is validated by simulation experiments.

Key words. Multidimensional, Subspace map identification, Aircraft, Fault-tolerant control.

1. Introduction

As a kind of optimal control algorithm with a strong industrial application background, model predictive control has the characteristics of good control performance, strong robustness, effective handling of multivariable restricted problems and so on, so it has been widely used in the process control for petroleum heavy industry , electric power and other fields.

The predictive control algorithm was first proposed for linear systems. When the object has a strong nonlinearity, the prediction and optimization have to be based on the Non-linear model, because the output prediction related to the linear

[1]College of Science, Shenyang Jianzhu University, Shenyang Liaoning, 110168, China

model is more deviated from the actuality and the goal of optimal control can not be achieved. At present, the nonlinear modeling methods that have been heavily studied include : mechanism model, Volterra model, Hammerstein model, Wiene model, etc. The establishment of mechanism model requires a thorough understanding of the controlled object, but the establishment of the mechanism model is often difficult if the production process is technologically complex and there are too many related factors. Volterra model, Harstein model, Wiene model and other special models require a wide range of device testing, so the cost of identification can be very high. Compared with linear MPC, nonlinear MPC has been rarely applied in industrial practice, and the biggest problem is the high cost of nonlinear process modeling and identification. Therefore, it is very important to find a Low-cost nonlinear modeling method.

In the past 20 years, subspace model identification (SMI) has received a great attention, not only due to its excellent convergence and the simplicity of numerical calculation, but also because it is more suitable to be applied for estimation, prediction and control algorithm. In the early references, most subspace identification methods have the characteristics of open-loop identification. With the Consideration of stability, safety and control-oriented identification problems, researchers have always been trying to apply these subspace methods to closed-loop identification. In the literature[9], The SubSpace method is extended to the estimation of the frequency response function, and the continuous and discrete time models are determined by auxiliary variables. In the literature [10], two frequency statistical characteristics and subspace convergence analysis method are presented.

For a linear closed-loop system in which the external input is not related to the observed noise, the cross-correlation function of the output and the external input signal is equal to that of the input that passes the dynamic system and the external signal . Therefore, the relationship between the two correlation function sequences can be completely determined and the unbiased parameter estimation can be obtained under arbitrary noise characteristics. The feature correlation function sequence is used as an interface function. The important information that it carries is hidden in the form of the compression correlation function in the data series, which provides the basis for the parameter identification by extracting the information about this parameter interface function .

In this paper, a subspace identification algorithm based on a new correlation function estimation is proposed specific to the morphing aircraft model identification, which can be used to obtain the unbiased parameter estimation under a dynamic closed-loop condition of a linear invariant system. The solution is to use the translational invariance of the dynamical system to realize the estimation of the correlation function.

2. Principle of magnetic field exploration of Quadrotor morphing aircraft

2.1. Operating principle of Quadrotor morphing aircraft

The traditional helicopter controls the flight direction by changing the propeller blade deflection, while the quadrotor morphing aircraft controls its flight direction by changing the rotational speed of its four propellers. In The following figure, it is assumed that the direction of the arrow is the direction in which the morphing aircraft advances. Fig. 1 shows how the propeller rotates when the morphing aircraft ascends vertically. The rotational speed of four propellers are increased simultaneously to produce a lifting drive to the fuselage, and the morphing aircraft is made to rise up vertically. When the quadrotor morphing aircraft needs to descend vertically, one just needs to reduce the rotational speed of the four propellers.

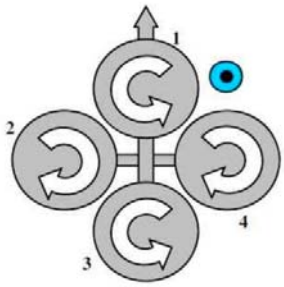

Fig. 1. How the propeller rotates during ascension

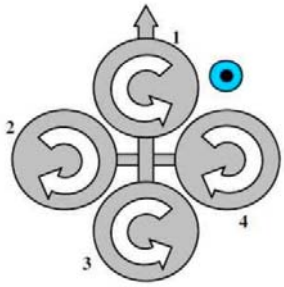

Fig. 2. How the propeller rotates when rolling towards the right

Figure 2 shows how the propeller rotates when the morphing aircraft rolls towards the right. Increase the rotational speed of 2, reduce the rotational speed of 4, keep the same speed of 1 and 3 , and make sure the sum of reverse torsion produced by the four propellers to the aircraft is zero, so that the morphing aircraft can be made to roll. To enable the morphing aircraft to make a pitching motion, one just needs to increase the rotational speed of 1 (or 3), decrease the rotational speed of 3 (or 1), and maintain the same rotational speed of 2 and 4, and make sure the sum of reverse torsion produced by the four propellers to the aircraft is zero.

2.2. Basis of dipole localization

Alternating current magnetic dipole is a small circular current of which the radius is a, the perimeter of the circle is far less than the wavelength λ, the amplitude and phase position of the time-harmonic current of the circle are the same everywhere. The magnetic dipole is a basic radiating element, also known as magnetic short dipole. According to the literatures, in the area close to the magnetic dipole, as r is very small, that is, $r \ll 1r \ll \lambda/2\pi$, the near zone field can be approximated as :

$$Hr = \frac{IS}{2\pi r^3}\cos\theta\,. \tag{1}$$

$$H_\theta = \frac{IS}{4\pi^3}\sin\theta\,. \tag{2}$$

The above formula is equivalent to $H = \frac{1}{4\pi}\frac{3(p\cdot n)n-p}{r^3}$, where I is the current value, S is the area of circle of magnetic dipole, $p = IS$, n is directional unit vector. When $r \gg a$ in the static magnetic field of magnetic dipole, The magnetic field distribution is:

$$B = \frac{\mu_0}{4\pi}[-\frac{p}{r^3} + \frac{3(p\cdot r)r}{r^5}]\,. \tag{3}$$

It is known from the distribution of alternating and static magnetic field of the magnetic dipole that, when $a \ll r \ll 2\pi/\lambda$, the alternating magnetic field can be equivalent to the static magnetic field, the magnetic field calculation formula is :

$$B = \frac{\mu_0}{4\pi}\frac{3(p\cdot n)n-p}{r^3}\,. \tag{4}$$

Assume a magnetic dipole exists at the origin of coordinates. Its dipole moment is denoted as p. assume r is a vector of the position where the three-dimensional pointing sensor is placed, then the magnetic induction intensity at where r is can be expressed as:

$$B = \frac{\mu_0}{4\pi}\frac{3(p\cdot n)n-p}{r^3}\,. \tag{5}$$

Where, $r = |r|$ denotes the far distance between the sensor and magnetic field. The magnetic field at where $r + ndr$ is is shown by Fig.3. it is easy to obtain:

$$B' = \frac{\mu_0}{4\pi}\frac{3(p\cdot n)n-p}{(r+dr)^3} \tag{6}$$

As the relation between n and p is the same as that between r and $r + ndr$, B' is parallel to B in direction, meanwhile, the value is inversely proportional to r^3 in

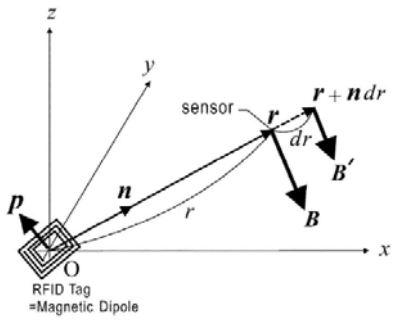

Fig. 3. Magnetic field differential relation

the direction of n. the total differential is :

$$\begin{aligned} B' - B &= \frac{\mu_0}{4\pi}(3(p\cdot n)n - p)(\frac{\partial}{\partial r}\frac{1}{r^3}dr) \\ &= -\frac{3}{r}\frac{\mu_0}{4\pi}\frac{3(p\cdot n)n - p}{r^3}dr = -\frac{3}{r}Bdr\,. \end{aligned} \tag{7}$$

On the other hand, the difference of vector B can be written in the form of magnetic field gradient as :

$$B' - B = \begin{bmatrix} \nabla B_x \cdot ndr \\ \nabla B_y \cdot ndr \\ \nabla B_z \cdot ndr \end{bmatrix} = \begin{bmatrix} \partial_x B_x & \partial_y B_x & \partial_z B_x \\ \partial_x B_y & \partial_y B_y & \partial_z B_y \\ \partial_x B_z & \partial_y B_z & \partial_z B_z \end{bmatrix} ndr\,. \tag{8}$$

It is solved that the location $r = nr$ is :

$$r = -3\begin{bmatrix} \partial_x B_x & \partial_y B_x & \partial_z B_x \\ \partial_x B_y & \partial_y B_y & \partial_z B_y \\ \partial_x B_z & \partial_y B_z & \partial_z B_z \end{bmatrix}^{-1} \begin{bmatrix} B_x \\ B_y \\ B_z \end{bmatrix}. \tag{9}$$

3. Closed-loop subspace identification based on correlation function estimation

By the correlation function estimation and the subsequently conducted null-space projection, the block matrix of the identification framework is filled, and the range of the extended observable matrix is obtained, which is the basic step of the subspace identification method. Then, the dynamic estimation of an unknown equipment system model can be obtained based on the same projection on the time offset set of the correlated data.

3.1. Block matrix data estimation equation

The block Hankel matrix of correlation function estimation $\hat{\boldsymbol{R}}^{yr}_{\tau_0|\tau_{i-1}}$ and $\hat{\boldsymbol{R}}^{ur}_{\tau_0|\tau_{i-1}}$ is built, including i rows and j columns, the specific definition is as follows:

$$\hat{\boldsymbol{R}}^{yr}_{\tau_0|\tau_{i-1}} = \begin{bmatrix} \hat{\boldsymbol{R}}_{yr}(\tau_0) & \hat{\boldsymbol{R}}_{yr}(\tau_1) & \cdots & \hat{\boldsymbol{R}}_{yr}(\tau_{j-1}) \\ \hat{\boldsymbol{R}}_{yr}(\tau_1) & \hat{\boldsymbol{R}}_{yr}(\tau_2) & \cdots & \hat{\boldsymbol{R}}_{yr}(\tau_j) \\ \vdots & \vdots & \ddots & \vdots \\ \hat{\boldsymbol{R}}_{yr}(\tau_{i-1}) & \hat{\boldsymbol{R}}_{yr}(\tau_i) & \cdots & \hat{\boldsymbol{R}}_{yr}(\tau_{j+i-2}) \end{bmatrix}. \tag{10}$$

$$\hat{\boldsymbol{R}}^{ur}_{\tau_0|\tau_{i-1}} = \begin{bmatrix} \hat{\boldsymbol{R}}_{ur}(\tau_0) & \hat{\boldsymbol{R}}_{ur}(\tau_1) & \cdots & \hat{\boldsymbol{R}}_{ur}(\tau_{j-1}) \\ \hat{\boldsymbol{R}}_{ur}(\tau_1) & \hat{\boldsymbol{R}}_{ur}(\tau_2) & \cdots & \hat{\boldsymbol{R}}_{ur}(\tau_j) \\ \vdots & \vdots & \ddots & \vdots \\ \hat{\boldsymbol{R}}_{ur}(\tau_{i-1}) & \hat{\boldsymbol{R}}_{ur}(\tau_i) & \cdots & \hat{\boldsymbol{R}}_{ur}(\tau_{j+i-2}) \end{bmatrix}. \tag{11}$$

Where, $\hat{\boldsymbol{R}}^{yr}_{\tau_0|\tau_{i-1}} \in \mathcal{R}^{n_y i \times n_r j}$, $\hat{\boldsymbol{R}}^{ur}_{\tau_0|\tau_{i-1}} \in \mathcal{R}^{n_u i \times n_r j}$. Each element of $\hat{\boldsymbol{R}}^{yr}_{\tau_0|\tau_{i-1}}$ and $\hat{\boldsymbol{R}}^{yr}_{\tau_0|\tau_{i-1}}$ are all correlation function data, i and j is the subscript defined by the user. According to formula (5), the above matrix meets the following relation:

$$\hat{\boldsymbol{R}}^{yr}_{\tau_0|\tau_{i-1}} = \Gamma \boldsymbol{R}^{xr}_{\tau_0} + \boldsymbol{T}_{0|i-1} \hat{\boldsymbol{R}}^{ur}_{\tau_0|\tau_{i-1}} \tag{12}$$

Where, the vector R^{xr}_{r0} is composed of the data of state cross-correlation function:

$$\boldsymbol{R}^{xr}_{r0} = \left[\boldsymbol{R}_{xr}(\tau_0)\boldsymbol{R}_{xr}(\tau_1)\cdots\boldsymbol{R}_{xr}(\tau_{j-1})\right]. \tag{13}$$

Then, the extended observable matrix and the lower triangular block Toeplitz matrix can be defined as :

$$\Gamma = \begin{bmatrix} \boldsymbol{C}_p & \boldsymbol{C}_p\boldsymbol{A}_p & \cdots & \boldsymbol{C}_p\boldsymbol{A}_p^{i-1} \end{bmatrix}^T. \tag{14}$$

$$\boldsymbol{T}_{0|i-1} = \begin{bmatrix} \boldsymbol{D}_p & 0 & \cdots & 0 \\ \boldsymbol{C}_p\boldsymbol{A}_p & \boldsymbol{D}_p & \cdots & 0 \\ \vdots & \vdots & \ddots & \vdots \\ \boldsymbol{C}_p\boldsymbol{A}_p^{i-2}B_p & \boldsymbol{C}_p\boldsymbol{A}_p^{i-3}B_p & \cdots & \boldsymbol{D}_p \end{bmatrix}. \tag{15}$$

Applying the single-step displacement process, the displacement equation to which the formula (10) corresponds can be defined as:

$$\hat{\boldsymbol{R}}^{yr}_{\tau_1|\tau_i} = \Gamma \boldsymbol{A}_p R^{xr}_{\tau_0} + \boldsymbol{T}_{0|i} \hat{\boldsymbol{R}}^{ur}_{\tau_0|\tau_i} \tag{16}$$

Where, the matrix $\boldsymbol{T}_{0|i}$ can be obtained by supplementing a column of null points

at the left side of $\boldsymbol{T}_{0|i-1}$, the form is as follows:

$$\boldsymbol{T}_{0|i} = \begin{bmatrix} 0 & \boldsymbol{D}_p & 0 & \cdots & 0 \\ 0 & \boldsymbol{C}_p\boldsymbol{A}_p & \boldsymbol{D}_p & \cdots & 0 \\ \vdots & \vdots & \vdots & \ddots & \vdots \\ 0 & \boldsymbol{C}_p\boldsymbol{A}_p^{i-2}\boldsymbol{B}_p & \boldsymbol{C}_p\boldsymbol{A}_p^{i-3}\boldsymbol{B}_p & \cdots & D_p \end{bmatrix}. \tag{17}$$

Similarly, the form of expression of $\hat{\boldsymbol{R}}^{ur}_{\tau_0|\tau_i}$ can be obtained by increasing a row of null points at the bottom of $\hat{\boldsymbol{R}}^{ur}_{\tau_0|\tau_{i-1}}$.

3.2. System dynamics estimation

The direct result that can be derived from Theorem 1 is that, as for the same projection $\prod^{ur}_{\tau_0|\tau_i}$, the projection at the right side of formula (5) and (8) can be used to remove the fixed term containing $T_{0|i-1}$ and $T_{1|i}$ from $\hat{\boldsymbol{R}}^{yr}_{\tau_0|\tau_{i-1}}$ and $\hat{\boldsymbol{R}}^{yr}_{\tau_0|\tau_i}$, then :

$$\hat{\boldsymbol{R}}^{yr}_{\tau_0|\tau_{i-1}} \prod{}^{ur}_{\tau_0|\tau_i} = \Gamma R^{xr}_{\tau_0} \prod{}^{ur}_{\tau_0|\tau_i}. \tag{18}$$

$$\hat{\boldsymbol{R}}^{yr}_{\tau_1|\tau_i} \prod{}^{ur}_{\tau_0|\tau_i} = \Gamma A_p R^{xr}_{\tau_0} \prod{}^{ur}_{\tau_0|\tau_i}. \tag{19}$$

Therefore, the estimation of extended observable matrix Γ **can be obtained through the singular value decomposition at the right side of formula (14), the calculation form is :**

$$\hat{\boldsymbol{R}}^{yr}_{\tau_0|\tau_{i-1}} \prod{}^{ur}_{\tau_0|\tau_i} = \begin{bmatrix} \boldsymbol{U}_n & \boldsymbol{U}_s \end{bmatrix} \begin{bmatrix} \sum_n & 0 \\ 0 & \sum_s \end{bmatrix} \begin{bmatrix} \boldsymbol{V}_n^T \\ \boldsymbol{V}_s^T \end{bmatrix} \tag{20}$$

$$\hat{\Gamma} = \boldsymbol{U}_n \sum_n^{1/2}. \tag{21}$$

According to the formula (20) and (21), the solution of least square to the minimization problem is as follows:

$$J = \arg\min_{\boldsymbol{A}_p} \left\| A_p \Gamma^{\dagger} \hat{\boldsymbol{R}}^{yr}_{\tau_0|\tau_{i-1}} \prod{}^{ur}_{\tau_0|\tau_i} - \Gamma^{\dagger} \hat{\boldsymbol{R}}^{yr}_{\tau_1|\tau_i} \prod{}^{ur}_{\tau_0|\tau_i} \right\|. \tag{22}$$

$$\hat{\boldsymbol{A}}_p = \sum_n^{-1/2} \boldsymbol{U}_n^T \hat{\boldsymbol{R}}^{yr}_{\tau_1|\tau_i} \prod{}^{ur}_{\tau_0|\tau_i} \boldsymbol{V}_n \sum_n^{-1/2}. \tag{23}$$

The system matrix C_p can be calculated by the use of n_y rows before the extended observable matrix, the specific form is :

$$\hat{\boldsymbol{C}}_p = \hat{\Gamma}\left(1 : n_y, :\right). \tag{24}$$

Based on the estimation of $\boldsymbol{A}_p$ and $\boldsymbol{C}_p$, the whole problem is turned into a linear one in the unknown $\boldsymbol{B}_p$ and $\boldsymbol{D}_p$. Then, the estimated form of output $\boldsymbol{y}(k)$ is:

$$\begin{aligned}\hat{y}(k) =&\hat{\boldsymbol{C}}_p\hat{\boldsymbol{A}}_p\hat{\boldsymbol{x}}(0) + (u(k)^T \otimes \boldsymbol{I}_{n_y})vec(\hat{\boldsymbol{D}}_p) \\ &+ (\sum_{t=0}^{k-1} \boldsymbol{u}(k)^T \otimes \hat{\boldsymbol{C}}_p\hat{\boldsymbol{A}}_p^{k-t-1})vec(\hat{\boldsymbol{B}}_p)\end{aligned} \tag{25}$$

Where, $\boldsymbol{B}_p$ and $\boldsymbol{D}_p$ can be estimated by solving the linear least square:

$$\min_{B_p,D_p} \frac{1}{N}\sum_{k=0}^{N-1} \left\|y(k) - \varphi^T(k)\theta\right\|_2^2 \tag{26}$$

where, $\varphi^T(k) = [(\boldsymbol{u}(k)^T \otimes \boldsymbol{I}_{n_y})(\sum_{k=0}^{s-1} \boldsymbol{u}(k)^T \otimes \hat{\boldsymbol{C}}_p\hat{\boldsymbol{A}}_p^{k-s-1})]$, $\boldsymbol{\theta} = [vec(\hat{\boldsymbol{D}}_p)\ \ vec(\hat{\boldsymbol{B}}_p)]^T$.

3.3. Algorithm step

The specific calculation process of the closed-loop subspace identification algorithm is shown in the Fig.4. firstly, the closed-loop prediction of parameter of matrix $\hat{\boldsymbol{L}}$ and $\hat{\boldsymbol{G}}$ of Γ are obtained based on the subspace projection method. Secondly, the calculated value of parameter $\hat{\boldsymbol{X}}$, $\boldsymbol{A}$, $\boldsymbol{C}$ and $\hat{\boldsymbol{R}}$ are obtained based on matrix operation and singular value decomposition, finally, the solution of system parameter matrix B and D are realized by least square.

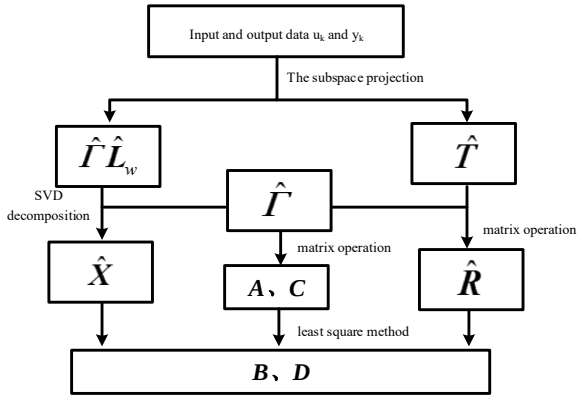

Fig. 4. Process of closed-loop subspace identification

In the Fig.4, $\hat{\Gamma}$ can be solved by calculation according to the formula (28), $\hat{\boldsymbol{L}}$ can be solved by calculation according to the formula (33-34), $\hat{T}$ can be solved by calculation according to the formula (16), $\hat{\boldsymbol{X}}$ is the state vector matrix of equipment, $\boldsymbol{A}$, $\boldsymbol{B}$, $\boldsymbol{C}$ and $\boldsymbol{D}$ are the process of calculation of state space matrix, for detail see the section 2.3: system dynamics estimation, $\hat{\boldsymbol{R}}$ can be solved by calculation according to the formula (35).

4. Experimental analysis

Apply the research result of this paper to the control and design of aircraft, the extra interference matrix is designed as:

$$R_i = [1, 0, \cdots, 0]^{\mathrm{T}}, D_d = [0.2, 0.4, 0.5, 0.3]^{\mathrm{T}} \tag{27}$$

To realize a non-linear dynamic scheduling, the convex function is defined as:

$$\rho_i(x(t)) = \frac{\mu_i(x(t))}{\sum_{i=1}^{3} \mu_i(x(t))}. \tag{28}$$

$$\mu_1(x(t)) = \exp\left[\frac{1}{2}\left(\frac{x_4(t) + 1.8}{0.8}\right)^2\right]. \tag{29}$$

$$\mu_2(x(t)) = \exp\left[\frac{1}{2}\left(\frac{x_4(t) - 1.8}{0.8}\right)^2\right]. \tag{30}$$

$$\mu_3(x(t)) = \exp\left[\frac{1}{2}\left(\frac{x_4(t)}{0.8}\right)^2\right]. \tag{31}$$

The attenuation level can be obtained by solving the deduction 1. the eigenvalue of observer is distributed within a circular region $\mathcal{D}(0.5, 0.5)$ of which the center is $(-0.5, 0)$ and radius is 0.5. The calculated attenuation level is $\gamma = 0.4965$. The form of calculation of parameter matrix P and Φ_3^{T} is shown in the table 1.

Table 1. The form of parameter matrix P and Φ_3^{T}

parameter matrix		1	2	3	4	5	6	7	8	9	10	11	12
Matrix P	1	0.39	-0.009	0	0	-0.0031	-0.000	-0.05	0.0009	0	0	0.002	0
	2	-0.009	0.84	0	0	0.0049	0.027	0.004	-0.1785	0	0.0049	-0.004	0
	3	0	0	2.48	0.0001	0	-0.00	0	0	-0.061	0.0001	0	-0.0
	4	0	0	0.001	2.49	0.0002	0.002	0	0	0.0001	-0.0001	-0.0003	-0.06
	5	-0.003	0.005	0	0.0002	5.62	-0.007	0.04	-0.006	0	-0.006	0.46	0
	6	-0.002	0.028	-0.0004	0.0002	-0.007	6.2508	0	-0.23	0.002	0.079	-0.014	0
	7	-0.056	0.04	0	0	0.04	0	0.174	-0.0002	0	0	-0.0005	0
	8	0.0009	-0.17	0	0	-0.0058	-0.22	-0.0002	0.23	0	-0.0137	0.0005	0
	9	0	0	-0.061	0.0001	0	0.002	0	0	2.3891	-0.0006	0	-0.
	10	0	0.004	0.001	-0.0001	-0.00	0.079	0	-0.0137	-0.0006	3.45	-0.004	0.004
	11	0.002	-0.004	0	-0.0003	0.46	-0.014	-0.0005	0.0005	0	-0.004	3.4	0.002
	12	0	0	-0.001	-0.0615	0	0.002	0	0	-0.0003	0.0004	0.0002	2.3
Matrix Φ_3^{T}	1	1.3492	-0.2873	-0.0001	-0.0005	0.0542	0.0368	-0.0401	-0.0311	0	0.0047	0.0051	0.0009
	2	-0.3713	1.0983	0	0.0006	-0.0042	-0.0472	0.0064	-0.0659	0.0001	-0.0003	-0.0055	-0.0006
	3	-0.0004	-0.0004	1.2812	0.0002	0.0035	-0.0046	0.0004	0.0003	0.0082	0.0042	0	-0.001
	4	-0.0002	-0.0003	0.0001	1.2822	-0.0008	-0.0084	0.0002	0.0007	0.0003	0	-0.0007	0.009

The observer gain matrix can be calculated as: $K_i = P^{-1}\Phi_i$. The matrix T_1 and T_2 can be calculated based on formula (21), besides, the observation eigenvalue of N_i is distributed in LMI area. The controller gain can be calculated by solving the deduction 2. Parameter of LMI area is taken as $\alpha = 1.5$. The calculated attenuation level is $\gamma_c = 0.4501$, which is small enough to ensure the desired control performance.

To prove the effectiveness of proposed method during fault, a group of 4 residual generators has been designed (each corresponding to an output), dual-sensor-induced fault is shown in the Fig.5e. the first fault happens to the second sensor, after $t = 45s$, it is a fault with deviant behavior. The second fault happens between $t = 12s$ and $t = 26s$, it is a sine performance fault happening to the 3^{rd} sensor. The normalized residual signal is shown in the Fig.5a∼d.

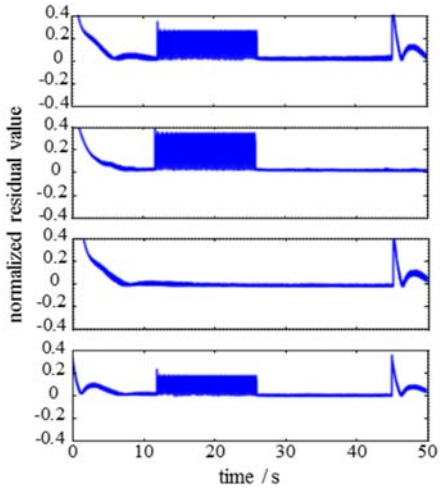

Fig. 5. Case of normalized residual fault

Fault detection can be easily done by comparing the residual error with the correlation matrix provided by the table 2. for example, as to the second fault happening to the third sensor, the residual error $r_1 r_2$ and r_4 change at $t = 12s$, only the residual error r_3 remains unchanged. Thus, it is possible to generate a specific signature $S = [1\ 1\ 0\ 1]^{\mathrm{T}}$. Then, by comparing the signature table 2, the faulted sensor 3 can be isolated. Obviously, the fault detection proves to be successful in all cases.

5. Conclusion

In this paper, a morphing aircraft system with the consideration of interference has been developed to realize the design of tracking controller and robustness fault diagnosis. The dynamic estimation of unknown equipment system model is obtained by using the same projection on the time offset set based on correlated data and the least square operation. In order to detect and isolate sensor fault, a set of observers

is used to generate a set of residual errors, so that each residual error is only sensitive to one fault. Each observer is designed to be interference-resistant. Then, with a simulation of a quad-rotor morphing aircraft, the developed method is proved to be suitable for the morphing aircraft. The simulation results show that the method is effective. Future research will focus on fault-tolerant control.

References

[1] X. Du, Y. Zhu, Z. Peng, Y. Cui, Q. Zhang, Z. Shi, Y. Guan, X. Sha, T. Shen, Y. Yang, X. Li, Z. Wang, X. Li, and G. Liu:*High concentrations of fatty acids and β-Hydroxybutyrate impair the growth hormone-mediated hepatic JAK2-STAT5 pathway in clinically ketotic cows.* J Dairy Sci *0302* (2018), No. 18,30029-8.

[2] Y. Y. Zhang, A. Algburi, N. Wang, V. Kholodovych, D. O. Oh, M. Chikindas, and K. E. Uhrich: *Self-assembled Cationic Amphiphiles as Antimicrobial Peptides Mimics: Role of Hydrophobicity, Linkage Type, and Assembly State*, Nanomedicine: Nanotechnology, Biology and Medicine *13* (2017) No. 2, 343–352.

[3] X. Du, S. Zhen, Z. Peng, C. Zhao, Y. Zhang, W. Zhe, X. Li, G. Liu, X. Li: *Acetoacetate induces hepatocytes apoptosis by the ROS-mediated MAPKs pathway in ketotic cows.* Journal of Cellular Physiology (2017) No./,232, 3296–3308.

[4] Y. Song, N. Li, J. Gu, S. Fu, Z. Peng, C. Zhao, Y. Zhang, X. Li, Z. Wang, X. Li: *β-Hydroxybutyrate induces bovine hepatocyte apoptosis via an ROS-p38 signaling pathway.* Journal of Dairy Science *99* (2016), No. 11, 9184–9198.

[5] N. Arunkumar, K. R. Kumar, V. Venkataraman: *Automatic detection of epileptic seizures using new entropy measures.* Journal of Medical Imaging and Health Informatics *6* (2016) No. refeq3, 724–730.

[6] R. Hamza, K. Muhammad, N. Arunkumar, G. R. González: *Hash based Encryption for Keyframes of Diagnostic Hysteroscopy*, IEEE Access, https://doi.org/10.1109/ACCESS.2017.2762405 (2017).

[7] D. S. Abdelhamid, Y. Y. Zhang, D. R. Lewis, P. V. Moghe, W. J. Welsh, and K. E. Uhrich:*Tartaric Acid-based Amphiphilic Macromolecules with Ether Linkages Exhibit Enhanced Repression of Oxidized Low Density Lipoprotein Uptake*, Biomaterials *53* (2015), 32–39.

[8] X. Sun, Y. Xue, C. Liang, T. Wang, W. Zhe, G. Sun, X. Li, X. Li, G. Liu:*Histamine Induces Bovine Rumen Epithelial Cell Inflammatory Response via NF-κB Pathway.* Cellular Physiology & Biochemistry *42* (2017), No. 3, 1109–1119.

[9] N. Arunkumar, V. S. Balaji, S. Ramesh, S. Natarajan, V. R. Likhita, S. Sundari: *Automatic detection of epileptic seizures using independent component analysis algorithm.* IEEE-International Conference on Advances in Engineering, Science and Management, ICAESM-2012, art (2012) No. 6215903, 542–544.

Received May 7, 2017